Effects of Charge Balance and Exciton Confinement on the Operational Lifetime of Blue Phosphorescent Organic Light-Emitting Diodes

Caleb Coburn and Stephen R. Forrest

Phys. Rev. Applied **7**, 041002 — Published 24 April 2017

DOI: 10.1103/PhysRevApplied.7.041002

Effects of charge balance and exciton confinement on the operational lifetime of blue phosphorescent organic light emitting diodes

Caleb Coburn[a] and Stephen R. Forrest[a,b]

[a]Department of Physics, University of Michigan, Ann Arbor, MI 48109

[b]Departments of Electrical Engineering and Computer Science, and Materials Science and Engineering, University of Michigan, Ann Arbor, MI 48109

Teaser

Charge balance and exciton confinement are keys to the efficiency and reliability of blue phosphorescent light emitting diodes (PHOLEDs), which are still too short-lived for many practical applications. In this work, both charge balance and exciton confinement over the lifetime of a blue PHOLED are directly measured. While there is some loss of exciton confinement in degraded devices, its effects are minor compared to intrinsic degradation of the emission layer.

Abstract

We measure the contribution of loss of charge balance and exciton confinement in the emission zone to the operational lifetime of blue phosphorescent organic light emitting diodes (PHOLEDs). Charge balance and exciton confinement are monitored as functions of time by measuring the emission intensity of either phosphorescent or fluorescent red emitting 'sensing' layers embedded within the charge transport layers outside of the emission zone. We find no significant change in charge balance over the lifetime of the device, while loss of exciton confinement accounts for <5% of luminance loss, confirming that degradation is primarily due to decomposition of molecular constituents within the emission layer of the PHOLED.

The reliability of phosphorescent organic light emitting diodes (PHOLEDs) is crucial to their usefulness in displays [1] and lighting [2]. Unlike that of red or green devices, the operational lifetime of blue PHOLEDs is too short for most practical applications. Studies of blue PHOLED lifetimes have focused primarily on degradation of the emission layer (EML) [3-6]; however the loss of luminance due to degradation in other layers may also contribute. For example, blue PHOLED lifetime is affected by changes in the charge balance efficiency, η_{CB}, defined as the ratio of excitons formed in the EML to the number of charges injected. Device lifetime is also affected by the loss of exciton confinement, η_{EC}, defined as the percentage of excitons generated in the EML that recombine without diffusing into adjacent layers. Thus, degradation of blocking layers, changes in layer morphology, or increased resistance can decrease the device luminous efficiency by reducing either η_{CB} or η_{EC}.

Here, we employ red, δ-doped (i.e. ultrathin) 'sensing layers' in the charge transport regions to monitor changes in η_{CB} and η_{EC} of a blue PHOLED over its operational lifetime [5,7,8]. Charge and triplet exciton leakage are distinguished by comparing the emission intensities from the fluorescent vs. phosphorescent sensing layers. Using this technique, we find that changes in exciton confinement accounts for <5% of luminance loss, while changes in charge balance do not contribute significantly. This confirms that degradation of molecular species primarily occurs within the emission layer itself.

To measure charge and exciton leakages from the EML, we fabricate devices having red-emitting phosphorescent or fluorescent sensor molecules doped into the electron (ETL) or hole transport layer (HTL). Assuming that phosphorescent sensing layers efficiently collect all leaked charges and excitons, the charge balance efficiency is determined from the ratio sensor emission to injected charges via

$$\eta_{CB}\eta_{EC} = 1 - \frac{q\Phi_p}{J\eta_{oc}\chi\Phi_{PLQY}}, \tag{1}$$

where q is the electron charge, J is the current density, Φ_p is the outcoupled photon flux emitted by the sensing layer, η_{oc} is the sensor layer optical outcoupling efficiency, χ is the fraction of emissive excitons (i.e. χ = 1 for a phosphorescent sensor and ¼ for a fluorescent sensor), and Φ_{PLQY} is the photoluminescent quantum yield of the sensor. Excitons formed in the EML rapidly intersystem cross on phosphorescent dopant molecules to form emissive triplets. Because triplet excitons on the fluorescent sensor are nonemissive at room temperature, fluorescent sensing layers only emit due to singlet excitons directly formed on the sensor by leaked charges or by Förster transfer from the EML. Hence, by preventing Förster transfer, fluorescent sensing layers are sensitive only to charge leakage. To quantify this leakage, we set $\eta_{EC} = 1$ in Eq. 1. Thus, phosphorescent sensing layers measure both charge and exciton leakage, while fluorescent sensing layers decouple these two by measuring charge leakage separately.

To avoid changing the device characteristics due to trapping of holes in the HTL or electrons in the ETL, sensor materials should have a deeper highest occupied molecular orbital (HOMO) energy (measured from the vacuum level) than the HTL, and a shallower lowest unoccupied molecular orbital (LUMO) energy than the ETL. Additionally, the sensing material luminescence should to be easily spectrally resolved from that of the dopant.

Three sensing devices: PtOEP-HTL sensing, PtOEP-ETL sensing, and DCM2-ETL sensing, were grown by vacuum thermal evaporation (VTE) at a base pressure $< 5 \times 10^{-7}$ torr on solvent-cleaned substrates comprising a pre-patterned, 70 nm thick indium tin oxide (ITO, 60 ± 10 Ω/sq.) layer on glass. The substrates were exposed to UV-ozone for 10 min immediately prior to loading into the VTE chamber. The 2 mm^2 device area is defined by the intersection of the ITO anode and the 100 nm thick Al cathode, the latter patterned by deposition through a shadow mask. The device structure for the PtOEP-ETL sensing device is: ITO anode / 10 nm hexa-azatriphenylene hexacarbonitrile (HATCN) hole injection layer (HIL) / 20 nm N,N'-bis(naphthalen-1-yl)-N,N'-bis(phenyl)-2,2'-dimethylbenzidine (NPD) HTL / 30 nm 4,40-bis(3-methylcarbazol-9-yl)-2,20-biphenyl (mCBP) doped 13 vol% with Ir (III) tris[3-(2,6-dimethylphenyl)-7-methylimidazo[1,2-f]-phenanthridine] ($Ir(dmp)_3$) EML / 6 nm mCBP hole and exciton blocking layer (HBL) / 30 nm Alq_3 ETL /1.5 nm 8-hydroxyquinolinato Li (Liq) electron injection layer (EIL) / cathode. The 2 nm thick Alq_3 layer immediately adjacent to the mCBP HBL is doped at 8 vol% with the red phosphor, Pt (II) octaethylporphine (PtOEP). The DCM2-ETL sensing device differs only by using a 0.05 nm thick layer of DCM2 located 10 nm distant from the EML. The structure for the PtOEP-HTL sensing device is the same as above except that the HTL consists of a 20 nm thick di(phenyl-carbazole)-N,N'-bis-phenyl-(1,1'-biphenyl)-4,4'-diamine (CPD) doped with a 0.1 nm thick PtOEP layer located 6 nm from the EML, with no sensor on the ETL side. Device structures are shown schematically in Fig. 1(a), along with the approximate transport levels of the materials. Each device has a single sensing layer, and in ETL sensing devices, CPD is replaced with NPD. The sensing layers are located sufficiently far from the EML to avoid direct Förster energy transfer from the blue dopant, Ir(dmp)$_3$. The transfer radii from Ir(dmp)$_3$ to PtOEP and DCM2 are 3.5 nm and 3.9 nm, respectively, calculated using the sensor absorption spectra in Refs. [9-11]. Layer thicknesses controlled using a crystal microbalance are accurate to within 5%.

PtOEP was chosen as the phosphorescent sensing material since its low triplet energy (E_T = 1.9 eV) allows efficient energy transfer from Alq$_3$ [12,13] (E_T = 2.1±0.1 eV). Also, its LUMO energy is aligned with that of Alq$_3$ [14] while the HOMO level (5.3±0.1) is approximately 0.5 eV higher than Alq$_3$ (5.8±0.2 eV). Hence, PtOEP traps holes but not electrons in the ETL [12,14]. On the other hand, CPD has a HOMO energy of 5.5 ± 0.1 eV and its LUMO energy is expected to be similar to NPD (~1.5 eV). Therefore, only electrons are trapped on PtOEP in CPD, with the PtOEP LUMO at 0.5 eV below that of the CPD, while the HOMO energies are aligned to within 0.2 eV, as shown in Fig. 1(a). The DCM2 HOMO is 5.3 eV, whereas its LUMO is 0.4±0.1 eV below that of Alq$_3$ and can trap electrons [15], although we find δ-doped layers cause no change in the device operating characteristics.

Following fabrication, the PHOLEDs are encapsulated in ultrapure nitrogen (<0.5 ppm oxygen and water concentration) using a glass slide sealed to the substrate with UV-cured epoxy applied around its periphery. The current-voltage-luminance characteristics of the packaged devices were measured immediately following fabrication. Two of each device type were life-tested at a current density of 30 mA/cm^2, and the electroluminescence spectra were measured at J=1 mA/cm^2 and 10 mA/cm^2 each time the devices degraded by approximately 5% of their initial luminance (at times corresponding to T100, T95, T90, etc.).

Films with the structures: 25 nm thick Alq_3 doped with 8 vol% PtOEP, 5 nm CPD / 0.1 nm PtOEP / 5 nm CPD / 0.1 nm PtOEP / 5 nm CPD, and 5 nm Alq_3 / 0.05 nm DCM2 / 5 nm Alq_3 / 0.05 nm DCM2 / 5 nm Alq_3 were deposited on quartz substrates for photoluminescent quantum yield (PLQY) measurements of the sensing layers. The measurements were carried out in an integrating sphere under nitrogen flow, and illuminated with a HeCd laser at a wavelength of 325 nm.

The PLQY of the PtEOP:Alq_3 film is 14.9 ± 1.6%; PtOEP:CPD film, 28.5 ± 1.9%; and DCM2:Alq_3 film, 50 ± 9%. The percentage of emissive excitons at the sensing layers that emit outcoupled photons is determined using Green's function methods [16] along with the indexes of refraction of the layers measured by ellipsometry. The percentage of outcoupled photons for the PtOEP-ETL sensing layer is $\eta_{oc}\Phi_{QY}\cdot 100\% = 2.3 \pm 0.2\%$; PtOEP-HTL, 5.1± 0.2%; and DCM2-ETL, 7.5 ± 1.4%.

The current density-voltage (*J*-*V*) characteristics of the PtOEP-ETL and PtOEP-HTL sensing devices, along with those for reference devices without sensing layers, are given in Fig. 1(b). The performance is similar for all device types, with small differences due to the different HTL materials used and unavoidable growth-to-growth variations. The DCM2-ETL sensing device J-V characteristic also is comparable to its reference. The peak external quantum efficiency of the devices was 8.8%. The luminance loss and voltage rise over time at $J = 30$ mA/cm^2 are given in Fig. 1(c) for the PtOEP HTL and ETL sensing devices. All devices show the same lifetime and voltage rise behaviors, independent of sensing layers employed.

The spectral evolution of the emission with time is given in Fig. 2. As the device ages, the emission intensity of the PtOEP-ETL sensing layer increases (Fig. 2(a)), whereas it decreases for the PtOEP-HTL sensing layer (Fig. 2(b)). The sensor intensity is obtained by subtracting the aged reference and sensing device spectra (Fig. 2, detail). Importantly, we estimate that at $J = 10$ mA/cm^2, the sensing layer emission is approximately two orders of magnitude below the point when every PtOEP molecule is excited. This site saturation limit is determined using $k_r N \approx \Phi_p/(\eta_{oc}\eta_\chi\Phi_{PLQY})$, where k_r is the radiative recombination rate and N is the number of sensor molecules. Due to the thin δ-doped sensor layers, care must be taken to avoid saturation which could occur at high current densities or for devices with poor charge balance due to the long (~100 μs) lifetime of PtOEP phosphorescence [17]. Unlike the PtOEP ETL sensing layer, the DCM2 ETL sensing emission does not change with device age, as shown in Fig. 2(c).

The fraction of charge injected to charge leakage from the EML is $1 - \eta_{CB}\eta_{EC}$, calculated using the phosphorescent sensing spectra, with results shown in Fig. 3. The leakage into the ETL, is shown in Fig. 3(a). It increases as the device ages, and is an approximately linear function of the fraction of loss in luminance (L) from its initial value (L_0), i.e. L/L_0. The differences in leakage at $J = 1$ mA/cm^2 and 10 mA/cm^2 are due to shifts in the charge recombination zone from the ETL to the HTL side of the EML with current [7]. This leads to proportionately larger sensor emission at low currents at the ETL side, whereas the HTL side leakage does not change over the same range of J (see Fig. 3(b)). Error bars reflect differences between similar devices.

Comparing the behavior of the sensor emission vs. aging time for the ETL sensing layers in Figs. 2(a) and 2(c), we see that the PtOEP emission increases while the DCM2 emission is constant. Because the DCM2 sensing data are only sensitive to charge leakage, we conclude that charge balance does not change as the device degrades. The increased emission from the PtOEP-ETL sensing layer is therefore attributed to increased leakage of triplet excitons into the ETL.

Exciton blocking at the EML/HBL interface relies on the high E_T = 2.95 eV of mCBP [18] relative to Ir(dmp)$_3$ (E_T = 2.7 ± 0.1 eV). A possible cause of the increased exciton leakage includes chemical degradation that results in low triplet energy degradation products in the HBL. Indeed, several degradation products of mCBP have been identified with smaller energy gaps and likely lower triplet energies than mCBP [19]. Alternatively, morphological changes of the blocking layers has been linked to degradation of organic photovoltaic devices, and could also play a role here [20]. For example, crystallite formation in the HBL can intermix the HBL and ETL layers, reducing their exciton blocking efficiencies.

Leakage into the HTL of analogous devices is attributed to exciton diffusion [7,21] that results from the low triplet energy of the HTL compared to the EML constituents. In addition, both NPD and CPD fluoresce in the wavelength range λ = 400-450 [21], which would be expected in the case of electron leakage into the HTL. This is not observed here, thus we conclude that emission from the HTL sensing layer is also due to exciton diffusion.

Quenching at defects reduces the lifetime and diffusion length of excitons within degraded EMLs. Additionally, increased nonradiative recombination of charges on defects reduces the exciton formation rate. These effects cause a decrease in the exciton flux into the HTL. We quantitatively determine the decrease in exciton flux by solving the diffusion equation together with the PHOLED degradation model based on hot triplet annihilation of Ref [4]. Specifically, we solve:

$$\frac{d}{dt}T(x,t,t') = \frac{d}{dx}\left[D(x)\frac{d}{dx}T(x,t,t')\right] + G(x,t') - \frac{1}{\tau(t')}T(x,t,t'), \tag{2}$$

where x is the position in the device, t is the time for triplet diffusion and transport (on the order of nanoseconds to microseconds), t' corresponds to the operation time leading to generation of defects (typically tens to thousands of hours), $T(x,t,t')$ is the triplet density, $D(x)$ is the diffusivity, $G(x,t')$ is the exciton generation rate normalized to that of the fresh device, and $\tau(t')$ is the exciton lifetime. The exciton density is zero at the sensing layer, corresponding to exciton trapping on sensor molecules, and excitons are blocked at the HBL. We use $D = 2.3\times10^{-7}$ cm^{2}s^{-1} and τ = 100 μs for exciton diffusion and lifetime in the HTL and 7.6×10^{-7} cm^{2}s^{-1} for the EML [7]. Values for $\tau(t')$ in the EML are obtained from Ref. [4] and range from 1.1 μs at L/L_0 =1.0 to 0.5 μs at L/L_0=0.16, with values intermediate to measurements obtained by linear interpolation. Finally, the dependence of G on t' is found by solving Eqs. (1-3) and (4d) of Ref. [4], simplified by assuming a uniform exciton generation zone, and using the corresponding parameter values given in Table 1, Ref. [4] for the hole and electron densities $p(t,t')$ and $n(t,t')$, respectively. The normalized exciton generation rate inside the EML is then $p(\infty,t')n(\infty,t')/[p(\infty,0)\ p(\infty,0)]$, and zero elsewhere. The exciton flux at the sensing layer is $D(x)dT(x,\infty,t')/dx$, evaluated at the position of the sensing layer.

The resulting change in exciton flux at the HTL sensor layer relative to the as-grown device is shown in Fig. 3 (dashed line), scaled to match the PtOEP HTL sensing data. The agreement between the HTL emission data and theory support the conclusion that reduced exciton leakage into the HTL results from reduced diffusion into the HTL due to EML degradation.

The contribution of loss of charge balance and exciton confinement to the luminance decrease is:

$$\Delta L_{CB}(t') = 100\% \times (1 - [\eta_{CB}(t')\eta_{EC}(t') - \eta_{CB}(0)\eta_{EC}(0)])/(1 - L/L_0), \qquad (3)$$

calculated using the PtOEP sensing data, with results shown in Fig. 4. Here, error bars represent the difference in $\Delta L_{CB}(t')$ calculated for similar devices. The loss of exciton confinement accounts for approximately 3% of luminance loss at J = 1 mA/cm^2, and 1-2% at 10 mA/cm^2. This implies 97% of luminance loss is due to degradation of molecular species in the EML itself, consistent with assumptions in previous work investigating the lifetime of blue emitting PHOLEDs [4,5,22].

In summary, we find that loss of exciton confinement contributes ~3% to the luminance loss in blue PHOLEDs over their operational lifetimes, while charge balance is not significantly changed. We reach this conclusion by direct measurement of the luminance from red-emitting sensing layers located within the electron and hole transport layers. Indeed, over 95% of the luminance loss in these devices occurs by direct aging of the dopants and/or hosts in the EML. The small loss of exciton confinement is attributed to chemical or morphological degradation of the HBL, while charge balance does not change significantly with aging. Based on these findings, further improvements in lifetime will require more robust hosts, emitters, or other strategies for reducing their degradation pathways [5,8,23,24].

Acknowledgements

The authors thank Jaesang Lee for helpful discussions, and for measurements of the HOMO energy of CPD by ultraviolet photoelectron spectroscopy, Yue Qu for assistance with the outcoupling calculations, and Tyler Fleetham for HOMO and LUMO energy measurements of mCBP and NPD by cyclic voltammetry. This work was supported by the Department of Energy Solid State Lighting Program (contract No. DE-EE000707), the Air Force Office of Scientific Research, and Universal Display Corporation.

References

[1] B. Geffroy, P. Le Roy, and C. Prat, Organic light-emitting diode (OLED) technology: materials, devices and display technologies, Polym Int **55**, 572 (2006).

[2] H. Sasabe and J. Kido, Development of high performance OLEDs for general lighting, J. Mater. Chem. C **1**, 1699 (2013).

[3] Q. Wang and H. Aziz, Degradation of Organic/Organic Interfaces in Organic Light-Emitting Devices due to Polaron-Exciton Interactions, ACS Appl. Mater. Interfaces **5**, 8733 (2013).

[4] N. C. Giebink, B. W. D'Andrade, M. S. Weaver, P. B. Mackenzie, J. J. Brown, M. E. Thompson, and S. R. Forrest, Intrinsic luminance loss in phosphorescent small-molecule organic light emitting devices due to bimolecular annihilation reactions, J. Appl. Phys. **103**, 044509 (2008).

[5] Y. F. Zhang, J. Lee, and S. R. Forrest, Tenfold increase in the lifetime of blue phosphorescent organic light-emitting diodes, Nat. Commun. **5**, 5008 (2014).

[6] H. Aziz, Z. D. Popovic, N. X. Hu, A. M. Hor, and G. Xu, Degradation mechanism of small molecule-based organic light-emitting devices, Science **283**, 1900 (1999).

[7] C. Coburn, J. Lee, and S. R. Forrest, Charge Balance and Exciton Confinement in Phosphorescent Organic Light Emitting Diodes, Adv Opt Mater **4**, 889 (2016).

[8] N. C. Erickson and R. J. Holmes, Investigating the Role of Emissive Layer Architecture on the Exciton Recombination Zone in Organic Light-Emitting Devices, Adv. Funct. Mater. **23**, 5190 (2013).

[9] A. K. Bansal, W. Holzer, A. Penzkofer, and T. Tsuboi, Absorption and emission spectroscopic characterization of platinum-octaethyl-porphyrin (PtOEP), Chem Phys **330**, 118 (2006).

[10] V. G. Kozlov, P. E. Burrows, G. Parthasarathy, and S. R. Forrest, Optical properties of molecular organic semiconductor thin films under intense electrical excitation, Appl. Phys. Lett. **74**, 1057 (1999).

[11] V. G. Kozlov, G. Parthasarathy, P. E. Burrows, V. B. Khalfin, J. Wang, S. Y. Chou, and S. R. Forrest, Structures for organic diode lasers and optical properties of organic semiconductors under intense optical and electrical excitations, Ieee J Quantum Elect **36**, 18 (2000).

[12] M. A. Baldo, D. F. O'Brien, Y. You, A. Shoustikov, S. Sibley, M. E. Thompson, and S. R. Forrest, Highly efficient phosphorescent emission from organic electroluminescent devices, Nature **395**, 151 (1998).

[13] H. D. Burrows, M. Fernandes, J. S. de Melo, A. P. Monkman, and S. Navaratnam, Characterization of the triplet state of tris(8-hydroxyquinoline)aluminium(III) in benzene solution, J. Am. Chem. Soc. **125**, 15310 (2003).

[14] A. J. Makinen, I. G. Hill, and Z. H. Kafafi, Vacuum level alignment in organic guest-host systems, J. Appl. Phys. **92**, 1598 (2002).

[15] F. Nuesch, D. Berner, E. Tutis, M. Schaer, C. Ma, X. Wang, B. Zhang, and L. Zuppiroli, Doping-induced charge trapping in organic light-emitting devices, Adv. Funct. Mater. **15**, 323 (2005).

[16] K. Celebi, T. D. Heidel, and M. A. Baldo, Simplified calculation of dipole energy transport in a multilayer stack using dyadic Green's functions, Opt. Express **15**, 1762 (2007).

[17] M. A. Baldo and S. R. Forrest, Transient analysis of organic electrophosphorescence: I. Transient analysis of triplet energy transfer, Phys. Rev. B **62**, 10958 (2000).

[18] H. Nakanotani, K. Masui, J. Nishide, T. Shibata, and C. Adachi, Promising operational stability of high-efficiency organic light-emitting diodes based on thermally activated delayed fluorescence, Sci. Rep. **3**, 2127 (2013).

[19] A. S. D. Sandanayaka, T. Matsushima, and C. Adachi, Degradation Mechanisms of Organic Light-Emitting Diodes Based on Thermally Activated Delayed Fluorescence Molecules, J Phys Chem C **119**, 23845 (2015).

[20] B. Song, Q. C. Burlingame, K. Lee, and S. R. Forrest, Reliability of Mixed-Heterojunction Organic Photovoltaics Grown via Organic Vapor Phase Deposition, Adv Energy Mater **5** (2015).

[21] K. Goushi, R. Kwong, J. J. Brown, H. Sasabe, and C. Adachi, Triplet exciton confinement and unconfinement by adjacent hole-transport layers, J. Appl. Phys. **95**, 7798 (2004).

[22] N. C. Giebink, B. W. D'Andrade, M. S. Weaver, J. J. Brown, and S. R. Forrest, Direct evidence for degradation of polaron excited states in organic light emitting diodes, J. Appl. Phys. **105**, 4 (2009).

[23] D. P. K. Tsang and C. Adachi, Operational stability enhancement in organic light-emitting diodes with ultrathin Liq interlayers, Sci. Rep. **6** (2016).

[24] T. B. Fleetham, L. Huang, K. Klimes, J. Brooks, and J. Li, Tetradentate Pt(II) Complexes with 6-Membered Chelate Rings: A New Route for Stable and Efficient Blue Organic Light Emitting Diodes, Chem Mater **28**, 3276 (2016).

Figure Captions

FIG. 1. (a) Schematic representation of devices. The energy levels of the organic layers, including the dopants and sensors are denoted inside the boxes, measured in eV from the vacuum level. Definitions of the acronyms used for each material are defined in text. Note that for the ETL-side sensing devices, the HTL is NPD rather than CPD. Each device contains a single sensing layer. (b) Current-density vs. voltage characteristics of the as-grown devices. Reference devices omit sensing layers but are otherwise unchanged. (c) Luminance (L) normalized to its initial value (L_0), and voltage rise (ΔV) vs. operating time at 30 mA/cm^2 for PtOEP-HTL and -ETL side sensing devices.

FIG. 2. (a) PtOEP electron transport layer (ETL) sensing device spectra. The intensity of the blue phosphorescent emission at wavelengths from 450 to 550 nm decreases with time while the sensor emission at 650 nm increases, indicating increasing exciton diffusion into the ETL. Data correspond to operating times of: 0, 0.1, 1.2, 3.3, 6.7, 11.4, 22.6, 39.5, 55.1, 71.7, 95.3, and 214 hours. (b) PtOEP hole transport layer (HTL) sensing device spectra. The sensing layer emission intensity decreases with time, indicating reduced leakage on the HTL side. Data correspond to operating times of: 0, 0.4, 1.5, 3.5, 8.0, 11.0, 16.4, 20.7, 30.1, 39.1, 59.2, 88.9, and 179 hours. (c) DCM2-ETL sensing device spectra. The intensity of the DCM2 emission is constant with time, indicating no change in hole penetration into the ETL. Data correspond to operating times of: 0, 0.3, 42.8, and 109 hrs. Sensor emission magnified by 30 X and vertically offset for clarity, is shown in the detail of (a)-(c).

FIG. 3. Percent leakage, $100\%(1-\eta_{CB}\eta_{EC})$, on (a) the ETL at J = 1 mA/cm^2 and 10 mA/cm^2, and (b) HTL sides of the blue phosphorescent organic light emitting device vs.

the percent luminance loss, L/L_0. The dashed line is a fit to the HTL side leakage. The HTL leakage decreases with time and is the same at both $J = 1$ and 10 mA/cm^2 (not shown). Error bars represent the differences between two samples of each device type.

FIG. 4. Percentage contribution of loss of charge balance and exciton confinement to luminance loss, $\Delta L_{\mathrm{CB}}(t')$, vs. the percentage of luminance loss, L/L_0, and operating time (top axis). Luminance loss is attributed to exciton leakage into the ETL, which accounts for 3% of the total loss in luminance of the blue electrophosphorescent device. At $J = 1$ mA/cm^2, the leakage is larger and increases more quickly than at 10 mA/cm^2.

Figures

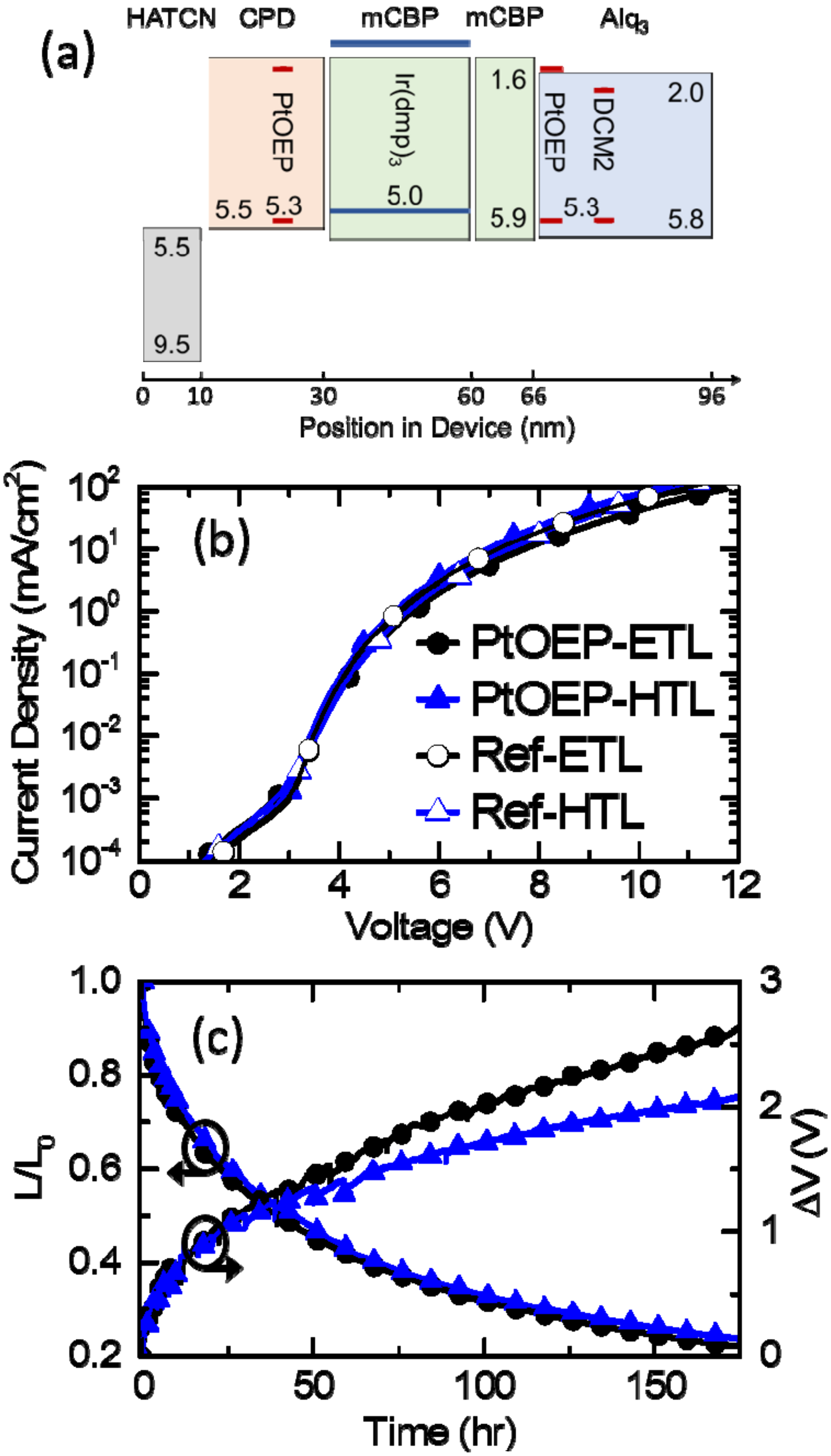
(a)
HATCN
CPD
mCBP
mCBP
Alq3
PtOEP
Ir(dmp)3
1.6
PtOEP
DCM2
2.0
5.5
5.3
5.0
5.9
5.3
5.8
5.5
9.5
0
10
30
60
66
96
Position in Device (nm)
(b)
Current Density (mA/cm2)
10^2
10^1
10^0
10^-1
10^-2
10^-3
10^-4
0
2
4
6
8
10
12
Voltage (V)
PtOEP-ETL
PtOEP-HTL
Ref-ETL
Ref-HTL
(c)
L/L0
1.0
0.8
0.6
0.4
0.2
ΔV (V)
3
2
1
0
0
50
100
150
Time (hr)

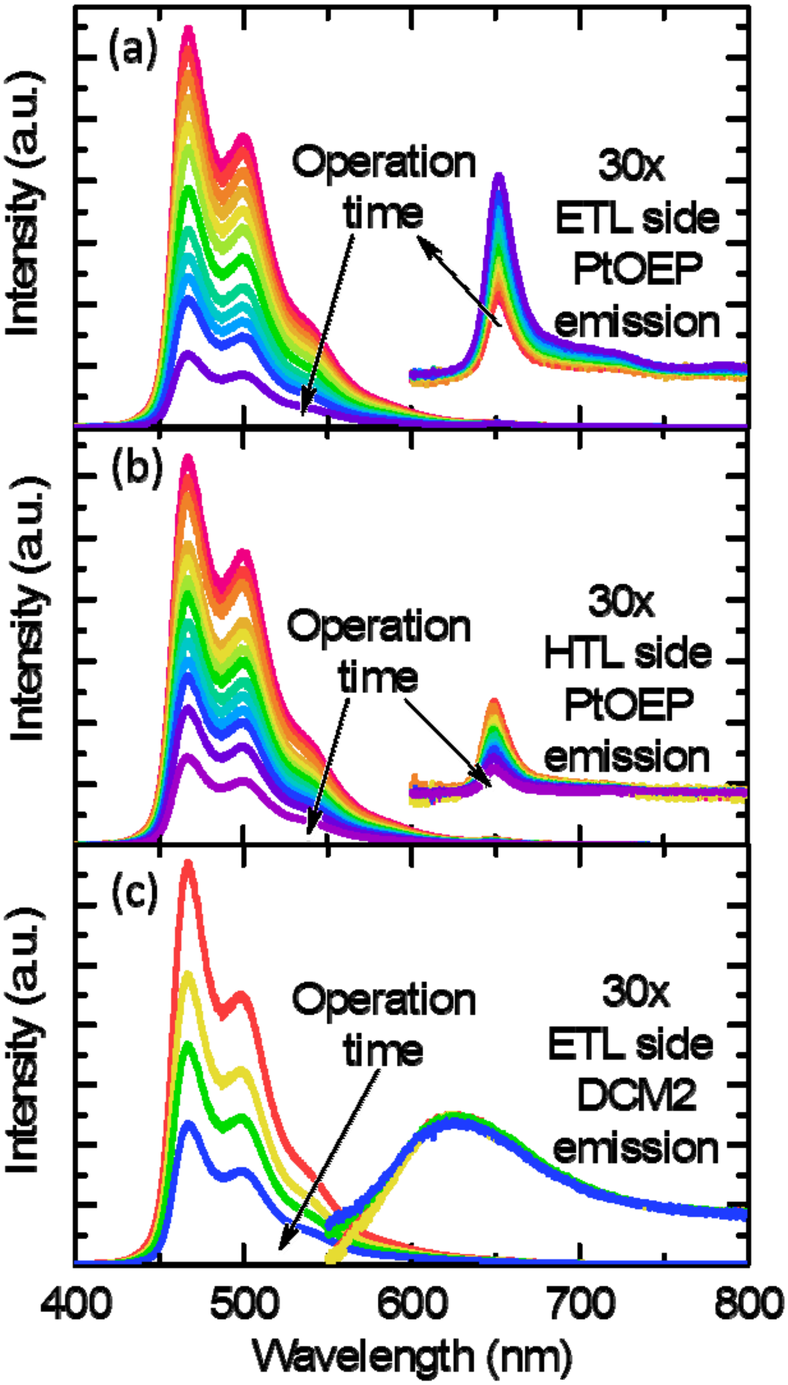
(a)
Intensity (a.u.)
Operation time
30x ETL side PtOEP emission
(b)
Intensity (a.u.)
Operation time
30x HTL side PtOEP emission
(c)
Intensity (a.u.)
Operation time
30x ETL side DCM2 emission
400
500
600
700
800
Wavelength (nm)

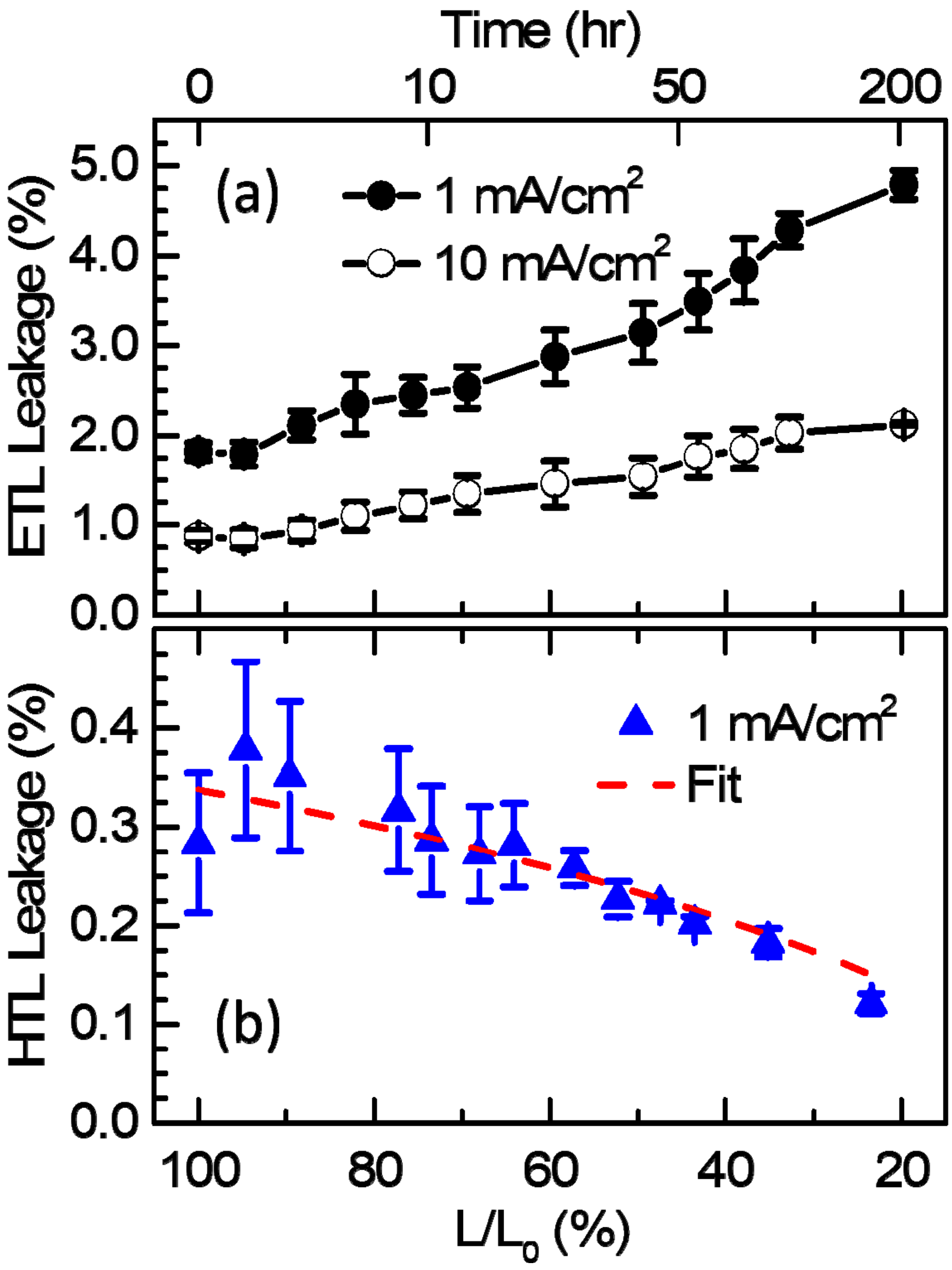
Time (hr)
0
10
50
200
(a)
1 mA/cm^2
10 mA/cm^2
ETL Leakage (%)
5.0
4.0
3.0
2.0
1.0
0.0
HTL Leakage (%)
0.4
0.3
0.2
0.1
0.0
1 mA/cm^2
Fit
(b)
100
80
60
40
20
L/L$_0$ (%)

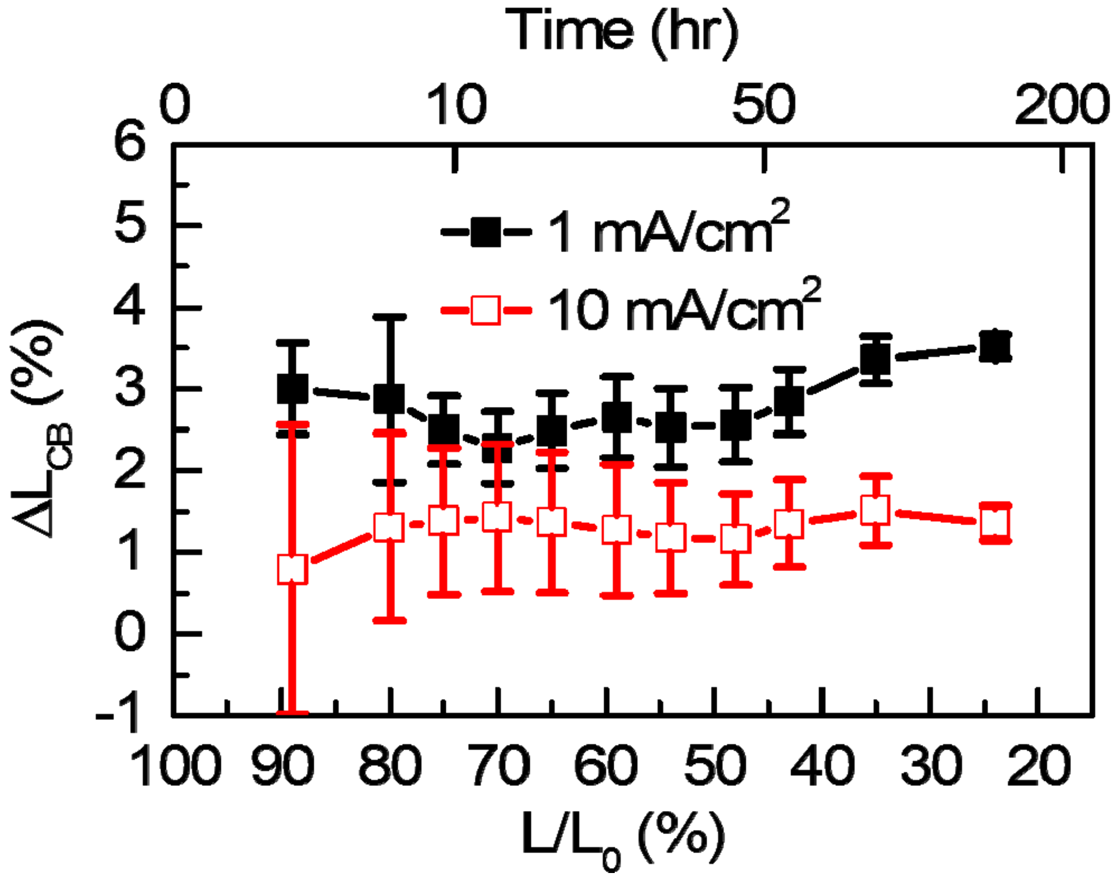
Time (hr)
0
10
50
200
6
5
4
3
2
1
0
-1
ΔL_{CB} (%)
1 mA/cm^2
10 mA/cm^2
100
90
80
70
60
50
40
30
20
L/L$_0$ (%)